

Experimental and numerical investigation of the effective electrical conductivity of nitrogen-doped graphene nanofluids

Mohammad Mehrali · Emad Sadeghinezhad · Mohammad Mehdi Rashidi · Amir Reza Akhiani · Sara Tahan Latibari · Mehdi Mehrali · Hendrik Simon Cornelis Metselaar

Received: 17 January 2015 / Accepted: 2 June 2015 / Published online: 13 June 2015
© Springer Science+Business Media Dordrecht 2015

Abstract Electrical conductivity is an important property for technological applications of nanofluids that have not been widely investigated, and few studies have been concerned about the electrical conductivity. In this study, nitrogen-doped graphene (NDG) nanofluids were prepared using the two-step method in an aqueous solution of 0.025 wt% Triton X-100 as a surfactant at several concentrations (0.01, 0.02, 0.04, 0.06 wt%). The electrical conductivity of the aqueous NDG nanofluids showed a linear dependence on the concentration and increased up to 1814.96 % for a loading of 0.06 wt% NDG nanosheet. From the experimental data, empirical models were

developed to express the electrical conductivity as functions of temperature and concentration. It was observed that increasing the temperature has much greater effect on electrical conductivity enhancement than increasing the NDG nanosheet loading. Additionally, by considering the electrophoresis of the NDG nanosheets, a straightforward electrical conductivity model is established to modulate and understand the experimental results.

Keywords Nitrogen-doped graphene · Nanofluid · Characterization · Stability · Electrical conductivity · Empirical models

M. Mehrali (✉) · A. R. Akhiani · S. Tahan Latibari · M. Mehrali · H. S. C. Metselaar
Department of Mechanical Engineering and Advanced Material Research Centre, University of Malaya, 50603 Kuala Lumpur, Malaysia
e-mail: mohamad.mehrali@siswa.um.edu.my

E. Sadeghinezhad (✉)
Department of Mechanical Engineering, University of Malaya, 50603 Kuala Lumpur, Malaysia
e-mail: esn802001@yahoo.com

M. M. Rashidi
Shanghai Automotive Wind Tunnel Center, Tongji University, 4800 Caoan Rd., Jiading, Shanghai 201804, China

M. M. Rashidi
ENN-Tongji Clean Energy Institute of Advanced Studies, Shanghai, China

Introduction

Energy transport is an integral part of a wide range of research areas, including chemical industry, oil and gas, nuclear energy, electrical energy, etc. In previous decades, ethylene glycol (EG), oil, and water were used as heat transfer fluids (Mehrali et al. 2014b; Sadeghinezhad et al. 2014). However, development of heat transfer fluids with improved thermal conductivity has become more and more critical to the performance of energy systems (Safaei et al. 2014). The convective heat transfer coefficients and pumping power requirements of fluids depend strongly on the Prandtl number and are highly influenced by viscosity and temperature of the fluid (Sadeghinezhad et al.

2014; Togun et al. 2014). On the other hand, dispersion of nanoparticles is a challenging task in the preparation of nanofluids and the nature of the surfactant plays a crucial role in the reaction mechanism. The first step towards preparation of a stable suspension was to find a suitable surfactant. Gum arabic (GA), sodium dodecyl sulfate (SDS), hexadecyltrimethylammonium bromide (CTAB), and Triton X-100 were used to produce aqueous nanofluids suspensions (Banerjee and Krupanidhi 2010). In addition, it can be noted that the importance of electrical conductivity characteristics of nanoparticle suspensions has largely been ignored in most studies and a few research works have been done on the electrical properties of nanofluids. It can be noted that most of the studies have typically investigated the mechanism of heat stability, thermal properties, and heat transfer characteristic of the nanofluids and their superior thermal performance over the conventional heat transfer systems.

Yet, apart from the thermophysical properties, the electrical conductivity might bring useful information on the state of dispersion and performance of the nanofluids (Ganguly et al. 2009). Electrical conductivity (σ) is the ability to conduct an electric current, which in a liquid solution is a liquid solution carried by anions and cations. Electrical conductivity is one of the important material characteristics for application in various fields and it is different and unique for each material and depends on the background electrolyte and particle size, charge, and concentrations. Recently, development of nanomaterials research has provided great changes in sciences and technology. Additionally, the electrical conductivity of nanofluids still remains poorly understood compared to the thermophysical properties of nanofluids (Chakraborty and Padhy 2008). The electrical conductivity of a suspension can either increase or decrease depending on the size, concentration, and background of electrolyte of nanoparticles. Electrical conductivity is normally measured in aqueous solutions of electrolytes, which can be either strong or weak and dependent on the temperature (White et al. 2011). Based on the surface and colloid theory, there is an electrical double layer (EDL) around each particle, which is a major factor in the colloidal stability of suspensions. The effect of EDL can be understood by the zeta potential, which is studied in the pH selection of the flotation process (Dong et al. 2013). The EDL

theory is useful in the explanation of the electrostatic and electrophoretic properties of suspensions. Some researches show that the electrical conductivity can affect the heat transfer properties of the nanofluids (electrical phenomena at interfaces: fundamentals: measurements, and applications 1998; Kalteh et al. 2011). The study of this property is important for applications which require electrically conducting fluids, including field-induced pattern formation in colloidal dispersions and electrically conducting adhesive technology.

The dispersed nanoparticles including ZnO, Cu, CuO, TiO₂, Al₂O₃, and CNT gain surface charge due to the protonation or deprotonation of a surface group such as a hydroxyl ligand (–OH) (White et al. 2011). The surface charge of nanoparticles can be adjusted by chemical treating of the nanoparticles surface or electrolyte solutions by altering the pH of the suspension. Several researchers have studied on the electrical conductivity measurements and found large enhancement in the electrical conductivity of nanofluids compared to the base fluid as the temperature concentration are increased (Cruz et al. 2005; Fang and Zhang 2005; Ganguly et al. 2009; Lisunova et al. 2006; Wong and Bhshkar 2006). Ganguly et al. (2009) found a factor of 150 for enhancement in electrical conductivity for Al₂O₃ nanofluids at a volume fraction of 3 %. Additionally, they found that the enhancement in electrical conductivity has a factor of 100 greater than the predicted value by the Maxwell model (Maxwell 1881; Maxwell and Thompson 1904). On the other hand, there are no available models for the electrical conductivity of nanofluids, and the researchers have simply used a linear curve fit without physical interpretation (Goharshadi et al. 2014; White et al. 2011). Kole and Dey (2013) have studied on the electrical conductivity of graphene nanofluid (70:30 mixture of DW and EG) and found that the electrical conductivity increased linearly with temperature and concentrations. Goharshadi and Azizi-Toupkanloo (2013) have measured the electrical conductivity of silver nanofluid and they observed 39.75 % increase in the electrical for a volume fraction of 2 % at 50 °C. Azizi-Toupkanloo et al. (2013) have measured the electrical conductivity of nanofluids of Pd/Ag NPs at different mass fractions and temperatures. They found that electrical conductivity of DW at 25 °C was increased 38.41 % when 1 % Pd/Ag NPs was added.

Recently, graphene is one of the amazing recent developments in modern science and one of the most promising materials for implementation in the next generation electronic devices (Usachov et al. 2011). Doping is a common approach to tailor the electronic properties of the semiconductor materials. For instance, after doping with N or B atoms, these semiconductor materials become n-type or p-type, respectively. Doping can also dramatically alter the electrical properties of graphene (Wei et al. 2009). Due to these reasons and based on the literature, NDG nanosheet has high electrical conductivity. On the other hand, little research have been done on the electrical conductivity of NDG nanofluids.

The objective of this work was to experimentally investigate the influence of nanosheet concentration and temperature on the electrical conductivity of aqueous NDG nanofluids. Recent reports have shown the effect of NDG roles in many technologies, industrial applications, and electrochemical devices such as batteries, super capacitors, etc. (Reddy et al. 2010). In the present work, the NDG synthesized by heat treatment of graphene in ammonia solution was followed by the preparation of stable nanofluids with desired characteristics. The present report contains results on the stability and electrical conductivity at different concentrations of the NDG nanofluids. Results are discussed to identify the mechanisms responsible for the electrical conductivity of NDG nanofluids prepared with different amounts of NDG nanosheets in distilled water (0.01, 0.02, 0.04, and 0.06 wt%) with Triton X-100 as a surfactant.

Materials and methods

Synthesize of nitrogen-doped graphene

A simplified Hummers' method was used to synthesize graphene oxide (GO) (Mehrali et al. 2013a, 2014a) and the NDG was prepared by a hydrothermal process with GO as raw material in an ammonia solution. As shown in Fig. 1, a mixture of 50 mg of GO and 100 mL of H₂O was sonicated for 1 h and pH of the solution was adjusted to 11 using ammonia. This homogenous solution was hydrothermally treated in a Teflon-lined autoclave at a temperature of 160 °C for 12 h. A black wooly precipitate was collected with

centrifugation, followed by washing with deionized water. Finally, the obtained NDG samples were dried at 50 °C under vacuum.

Nanofluid preparation

Water is a common heat transfer fluid. However, NDG cannot be directly dispersed in water, as there is no chemical affinity between them. Mixing of these materials directly leads to non-uniform suspensions and sedimentation of NDG starts almost immediately. Dispersion of NDG is a challenging task in the preparation of nanofluids. The nanofluid should be a stable and an agglomerate-free suspension without sedimentation for a long duration. In this experiment, the most effective surfactant and sonication time were selected by examining the stability of nanofluids. The first step towards preparation of a stable suspension was to find a suitable surfactant. According to previous research (Yousefi et al. 2012), surfactant and sonication time are important parameters for dispersing the nanosheet. Based on Yousefi et al.'s (2012) study, Triton X-100 as a non-ionic surfactant is the best dispersing agent for carbon-based nanoparticles due to the presence of benzene ring. This benzene ring is adsorbed on the NDG surface due to π - π stacking. In this, Triton X-100 could help nanosheet dispersion by forming a large solvation shell around them. The optimized parameters for the NDG nanofluid preparation were 60 min ultrasonication (probe) and 0.025 wt% aqueous solution of Triton X-100 as a surfactant, and then the concentrations of nanofluids were maintained at 0.01, 0.02, 0.04, and 0.06 wt%.

Measurements procedure of the electrical conductivity

In this experiment, measurements of the electrical conductivity were carried out both as a function of nanosheet concentration and temperature. In this experiment, the electrical conductivity was measured using a bench type of electrical conductivity meters. The electrical conductivity measurements of NDG nanofluid were conducted to examine the effects of variations in the temperature range from 25 to 60 °C and concentration between 0.01 and 0.06 wt%. For each case, six measurements were performed, and the mean value was reported.

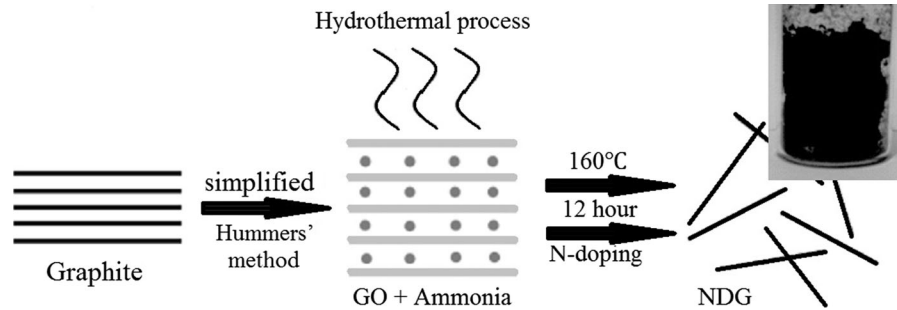


Fig. 1 Schematic illustration of nitrogen-doped graphene synthesis

Analysis methods

Field emission scanning electron microscopy (FESEM-CARL ZEISS-AURIGA 60) was used to observe the microstructure of the NDG. Transmission electron microscopy (TEM) measurements were conducted on a CARL ZEISS-LIBRA120 microscope. An X-ray photoemission spectrometer (PHI-Quantera II) with an Al- $K\alpha$ ($h\nu = 1486.8$ eV) X-ray source was used to identify bonding of the elements in the NDG. X-ray diffraction (XRD) patterns were measured on the Empyrean PANALYTICAL diffractometer. Raman spectra were obtained using a Renishaw Invia Raman Microscope using laser excitation at 514 nm. Atomic force microscopy (AFM, Bruker- MultiMode 8) in tapping mode was used to show the size of GO and NDG. Fourier transform-infrared (FT-IR) absorption spectra of the composites were recorded using a Bruker FT-IR (Bruker Tensor 27) spectrometer at room temperature in the range $4000\text{--}400$ cm^{-1} using ATR mode. The Brunauer–Emmett–Teller method (BET-Autosorb-iQ2) was used to measure specific surface area and pore distribution of the NDG sample. The weight loss and thermal stability of PCMs are obtained by thermogravimetric analysis (METTLER TOLEDO SDTA 851-Error ± 5 μg) at a heating rate of 10 $^{\circ}\text{C}/\text{min}$ and a temperature of $50\text{--}500$ $^{\circ}\text{C}$ in purified nitrogen atmosphere. The zeta potential of the nanofluids was measured on a Zetasizer nano (Malvern Instruments Ltd., United Kingdom). The rheological behavior of nanofluids with amounts of NDG was measured on Anton Paar rheometer (Physica MCR 301). A transient heated needle (KD2 Pro, Decagon Devices, Inc., USA) was used to measure the thermal conductivity with 5 % accuracy at a constant temperature. The thermal conductivity measurements

are repeated ten times and the average values were reported. The electrical conductivity was measured using AB200 pH/Conductivity Meter (Fisher Scientific). The light transmission of all samples was measured with a Cary 50 UV-Vis spectrophotometer, Agilent Technologies that is operating between 200 and 1100 nm.

Results and discussion

Characterization of nitrogen-doped graphene

The FESEM image in Fig. 2 shows a uniform structure like a crumpled silk veil with porous and worm-like structures, while silk-like transparent NDG nanosheets are randomly stacked together. It could be observed that the two-dimensional graphene structures with high volume ratio and specific surface area are well retained after hydrothermal treatment with ammonia.

The specific surface area of the NDG sample was measured and the graph is shown in Fig. 3. The unique mesoporous structure of NDG contributes to the high specific surface area (793 m^2/g) which is higher than our prepared GO (684 m^2/g) with a uniform pore size distribution around 3–5 nm. Over the synthesis of NDG sheets, besides the carbon atoms that were replaced by nitrogen atoms (most likely located on the reactive edge), ammonia can also react with graphene to form hydrogen cyanide and hydrogen ($\text{C} + \text{NH}_3 = \text{HCN} + \text{H}_2$).

The XRD patterns for the NDG and GO are shown in Fig. 4. Crystalline materials generally have well-defined XRD peaks, while amorphous materials result in a broad body ground with shallow peaks. The GO has a strong (001) peak at $2\theta = 9.71^{\circ}$ and d -spacing is

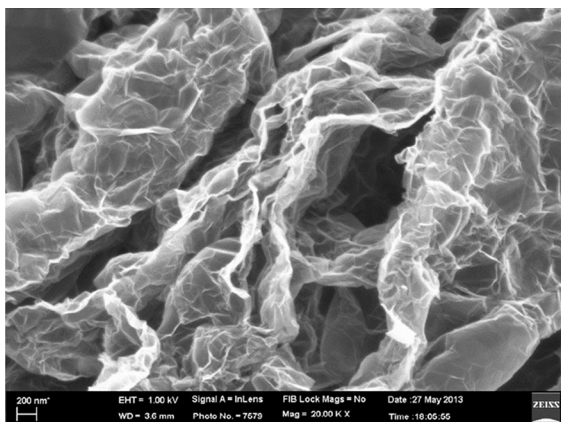


Fig. 2 FESEM image of NDG nanosheets

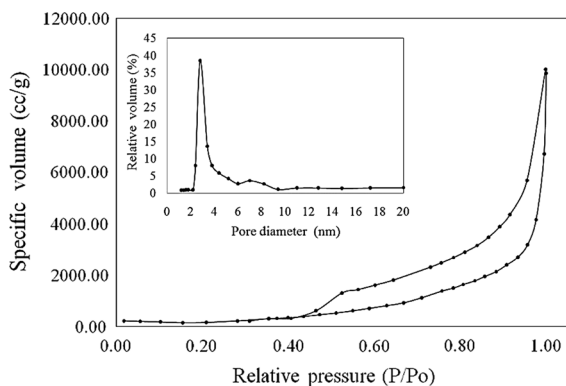


Fig. 3 Nitrogen adsorption/desorption isotherms of NDG. *Inset* is the BJH pore size distribution

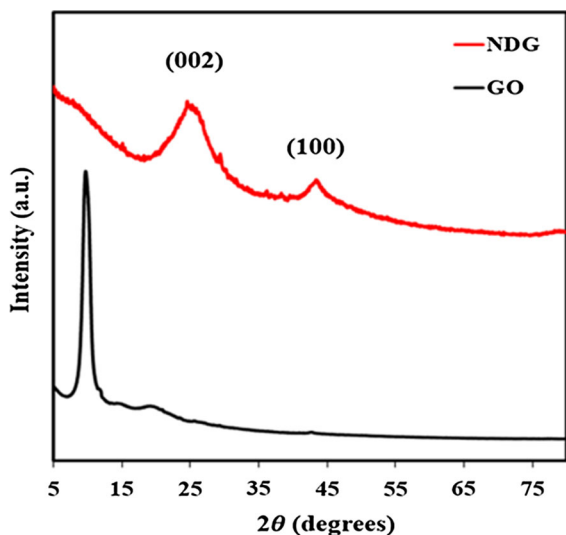


Fig. 4 XRD patterns of GO and NDG

0.91 nm, which is the preferred orientation of GO basal planes parallel to the sample plane (Blanton and Majumdar 2012; Liu et al. 2014).

In the XRD pattern for the NDG observed a peak at $2\theta = 24.5^\circ$ corresponding to the (002) graphitic inter-layer spacing, and another peak at $2\theta = 44^\circ$, corresponding to the (100) in-plane hexagonal atom arrangement. The NDG peaks are fairly small and broad, reflecting the defective nature of NDG, as well as the highly porous nature. It shows that only a few layers are stacked together, which result in a very low inter-layer spacing signal (Blanton and Majumdar 2012; Liu et al. 2014).

More descriptive details about its morphology were obtained from TEM. As can be observed in Fig. 5, NDG nanosheets were built with a regular crumpled surface with random stacking, which can be caused by the defective structure formed after exfoliation as well as the presence of foreign nitrogen atoms (Sheng et al. 2011). The very well-identified SAED spots and rings (inset of Fig. 5) showed a distinct hexagonal lattice, confirming the crystalline structure of NDG, but were slightly different from those of the specific graphene sheets due to doping and overlapping (Hernandez et al. 2008).

The single-sheet characteristics of the GO obtained were validated by AFM (Fig. 6). The thickness from the graphene sheet obtained was around 0.8 nm, corresponding well with the reported apparent thickness of single-sheet graphene. Although there are sporadic multilayers in NDG, the AFM image demonstrates that NDG is uniform with an apparent thickness of about 1.8 nm (Fig. 6b), suggesting NDG is a few-layer film.

FT-IR spectra were then used to analyze the chemical compositions of GO and NDG (Fig. 7). The main peaks in FT-IR spectrum of GO centered at 1046, 1221, 1412, 1631, 1728, and 3400 cm^{-1} can be attributed to alkoxy C–O, epoxy C–O and C–OH, carboxyl O=C–O, aromatic C=C, C=O (carboxylic acid and carbonyl moieties), and O–H stretches, respectively, confirming the successful oxidation of graphite (Mehrali et al. 2013b). After solvothermal treatment, the content of these oxygen-containing groups in GO significantly decreased, while two new nitrogen-related peaks shown up at 1458 and 1550 cm^{-1} in the FT-IR spectrum of NDG, which can be preliminarily assigned to C–N stretching and N–H bending bonds of amide, respectively (Wu et al. 2012).

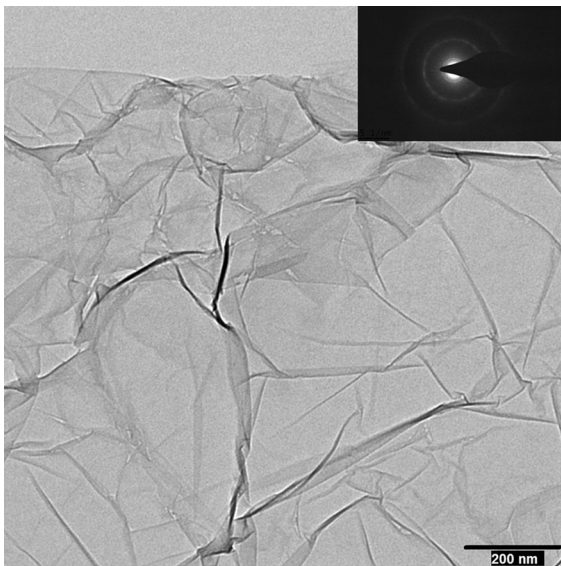


Fig. 5 TEM image of NDG and the corresponding SAED pattern (*inset*)

To help investigate the elemental composition and nitrogen bonding configurations in NDG, XPS measurements were performed. As shown in Fig. 8, there are three peaks centered at 284.2, 399.3, and 532 eV, which are related to C1s, N1s, and O1s, respectively,

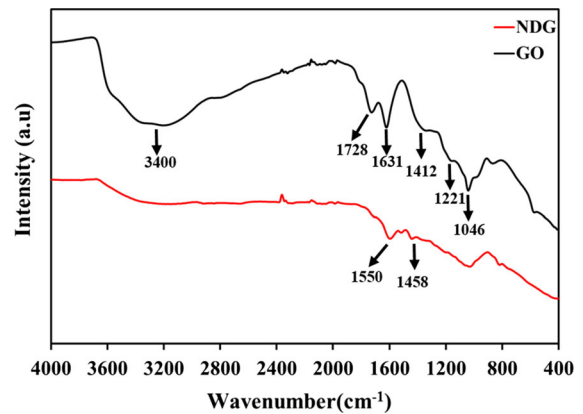


Fig. 7 FT-IR spectra of GO and NDG

and this shows that the incorporation of nitrogen within the graphene (Guo et al. 2013; Reddy et al. 2010).

The original GO has quite high oxygen content (38.3 %). Upon hydrothermal reduction, the carbon content raises up to 89.2 %, which is at the expense of the excellent reduction of oxygen content. This result suggests that the oxygen functionalities are actually eliminated mostly. It must be noted that the nitrogen content was zero within the initial GO, that was increased up to 2.64 % in NDG structure.

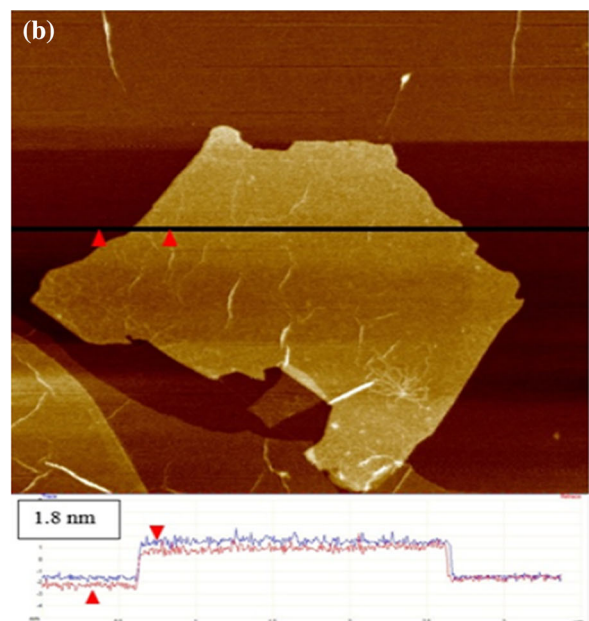
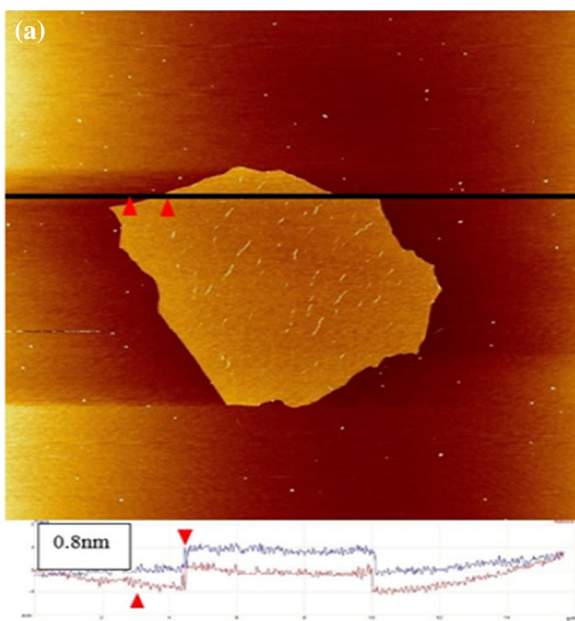


Fig. 6 AFM image of **a** GO and **b** NDG with corresponding height profile

Figure 9 shows the C1s XPS spectra of GO and NDG. The full width at half maximum (FWHM) of NDG appeared to be narrower following reduction, suggesting an increased graphitic degree. A substantial level of oxidation was noticed in GO, related to the carbon atoms in various functional groups: C–C (284.7), C–O (286.9), C=O (288.1), and COOH (288.7 eV) (Mehrali et al. 2014d). Considerably, the peak intensities of oxygen-containing groups became considerably weaker in NDG, while it can be noticed that an additional peak showed up at 285.9 eV, which can be assigned to the C–N bonds (Long et al. 2010).

The high-resolution N1s XPS spectrum of NDG was then compiled in Fig. 10a. Generally, the peaks located at 398.2, 400.3, and 403.8 eV are assigned to pyridinic-, pyrrolic-, and graphitic-forms of nitrogen atoms doped within the graphene structure, respectively (see Fig. 10b) (Mehrali et al. 2014c). It might be normally recognized that the covalent functionalization with amino groups may appear at the edge or defect sites of GO over the reduction process with ammonia; thus, the peak centered at 399.8 eV could be assigned to amino nitrogen atom (Lin et al. 2010), which is in conjunction with the previous FT-IR result. FT-IR and XPS spectra can support that the pristine GO was properly reduced and successfully doped/modified with nitrogen atoms/amino group as a result of low-temperature solvothermal process, producing NDG successfully.

Raman spectroscopy is a powerful non-destructive technique to study carbonaceous materials including

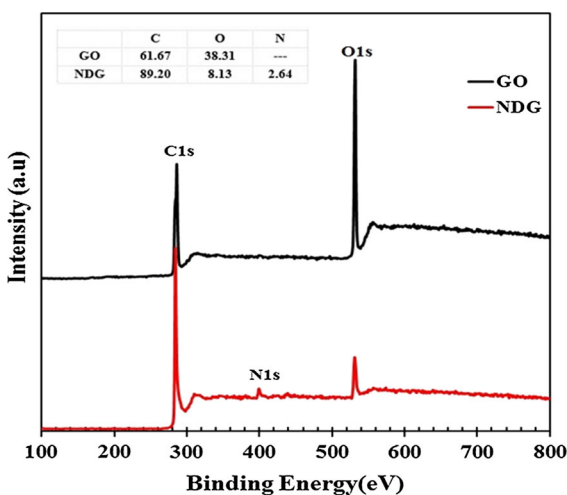


Fig. 8 Low-resolution XPS spectra of GO and NDG

graphene. Raman characteristics of carbon materials are the G bands ($\sim 1580\text{ cm}^{-1}$) and D bands ($\sim 1350\text{ cm}^{-1}$) (Akhavan and Ghaderi 2012). The G bands are associate with the E_{2g} phonon of $C\text{ sp}^2$ atoms and the D bands are breathing mode of k -point phonons of A_{1g} symmetry and are associated with local disorder and defects especially at the edges of graphene and graphite platelets (Akhavan 2010). Figure 11 shows the Raman spectra NDG and GO. The Raman spectrum for NDG gives two prominent peaks at 1354 and 1581 cm^{-1} , which correspond to the D and G bands, respectively. Figure 11 shows the G line at about 1588 cm^{-1} and the D line at 1355 cm^{-1} for the GO. The intensity ratio between the G band and D band (I_D/I_G) ratios for the samples GO and NDG were 0.77 and 0.94, respectively. This shows that the nitrogen doping can make a lot of defects in the graphene structure, which can contribute to a high-intensity D band (Vinayan and Ramaprabhu 2013). Moreover, the 2D band ($\sim 2700\text{ cm}^{-1}$) can be used to distinguish graphene with different layers. A broader and up-shifted 2D peak, compared to the spectrum of single-layer graphene, indicates that the NDG is predominantly a few-layer graphene that was confirmed by AFM results.

The mass loss of GO was close to 5 % at around $100\text{ }^\circ\text{C}$, which is assigned to the elimination of water molecules captured within the GO structure (see Fig. 12). An instant mass loss of 20 % taking place around $200\text{ }^\circ\text{C}$ is attributed to the pyrolysis of the labile oxygen-containing groups in the forms of CO, CO₂, and steam. NDG reveals an extremely higher residue than GO. The main mass loss of NDG at $130\text{--}210\text{ }^\circ\text{C}$ is because of the decomposition of residual oxygen-containing groups and $\text{N}(\text{CH}_3)_2^+$ groups.

Stability evaluation of nitrogen-doped graphene nanofluid

The stability of the nanofluid was determined by measuring the sediment time by the UV–Vis spectrophotometer as is widely done in evaluating the relative concentration of the nanofluids. UV–Vis spectrophotometer method is based on Beer–Lambert’s law, which states that the absorbance was directly proportional to the concentration of the nanosheet in the nanofluids.

Figure 13a shows the UV–Vis spectrophotograph of NDG colloidal suspension in DW. The maximum

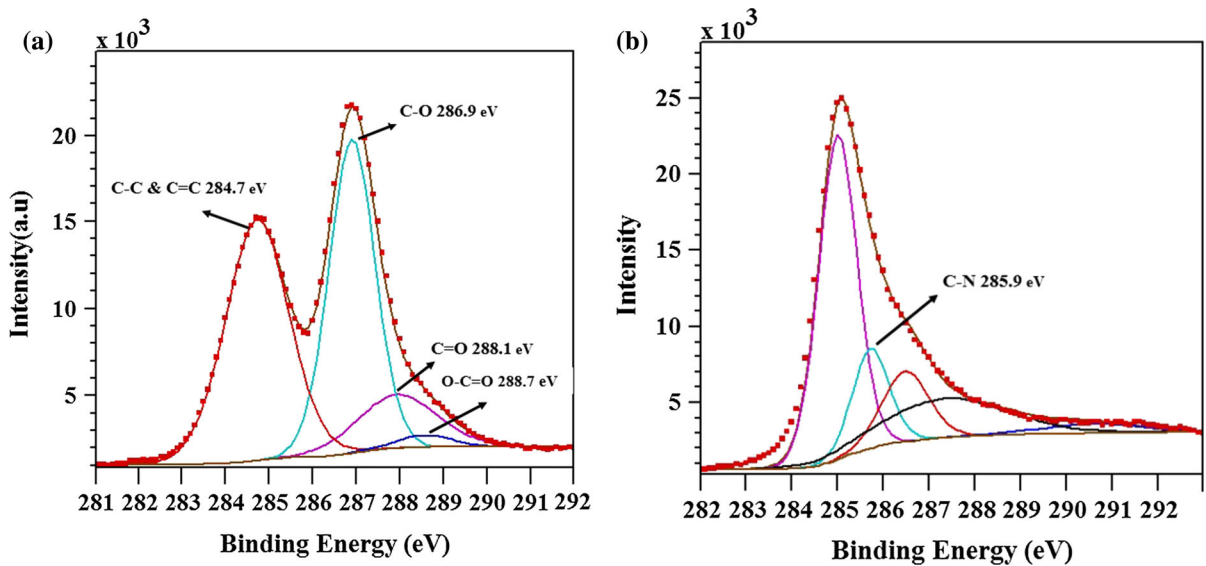


Fig. 9 The C1s XPS spectra of **a** GO and **b** NDG

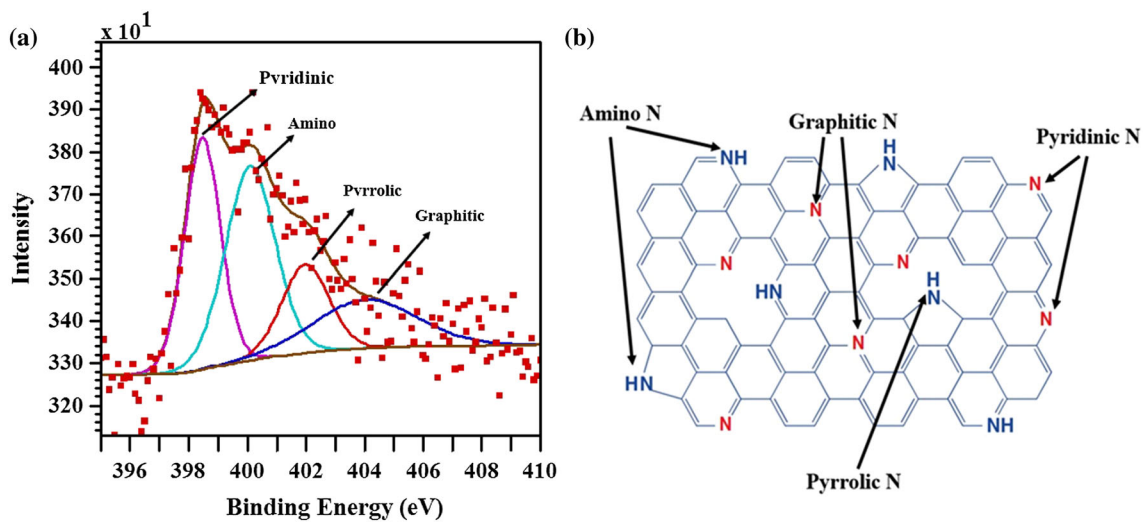


Fig. 10 **a** The N1s XPS spectrum of NDG and **b** schematic illustration of NDG. The various 'N' atoms represent the pyridinic N, pyrrolic N, graphitic N, and amino group in graphene structure

linear absorption wavelength is located at 275 nm, which is the same for all concentrations. It can satisfy Beer's law and indicates that NDG was dispersed well in the base fluid. It shows that the suspension can be considered as a stable nanofluid. It also shows that the characteristic bands corresponding to additional absorption are due to the 1D van Hove singularities (Aravind et al. 2011). To measure the relative concentration of the suspensions with the sediment

time, the same sample of DW and NDG nanofluids was used as a reference to eliminate the absorbance of nanofluid.

The dispersed nanosheet in the base fluids was influenced by gravity, as well as by particle–particle and particle–fluids interactions (Mehrali et al. 2014b). Therefore, the concentration of the nanofluids changes from the initial state of preparation and it is important to study the stability of the nanofluids. Figure 13b

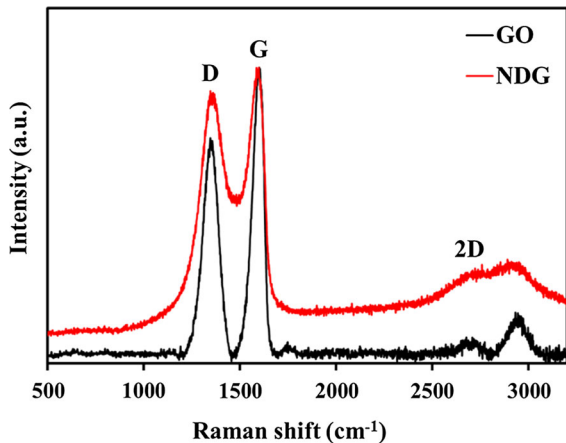


Fig. 11 Raman spectra of GO and NDG

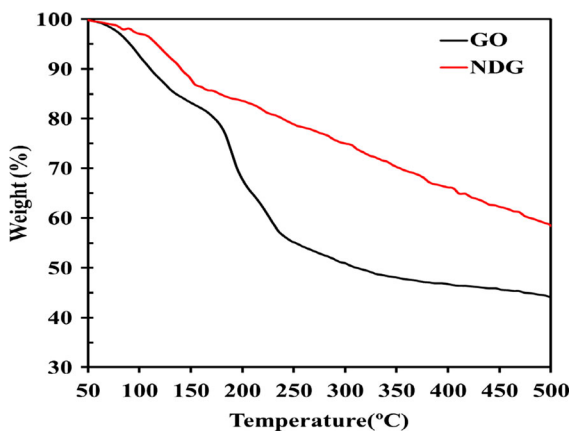


Fig. 12 TGA curves of GO and NDG

shows the colloidal stability of the NDG nanofluids during 200 days. The concentration of NDG nanofluids was decreased, which was attributed to sedimentation and particle agglomeration after long periods. Figure 13b shows that the relative concentration of nanofluid at 0.01 wt% was almost steady for 200 days. It shows that the colloidal stability of the NDG nanofluids for the concentrations of 0.02, 0.04, and 0.06 wt% remains relatively constant and was only reduced by 10, 16, and 20 %, respectively.

The colloidal stability of NDG nanofluids could be predicted from the zeta potential values of the nanosheet dispersed in DW, which closely related to its electrophoretic properties of nanofluids. A well-dispersed suspension can be obtained with a zeta potential of more than +30 mV or less than -30 mV

(high surface charge density) to generate strong repulsive forces (Mehrali et al. 2014b). The zeta potential value at pH 8 is -46.3 mV, which is in line with the excellent stability found by UV-Vis studies (Mehrali et al. 2014b). Additionally, the particle size distribution of nanosheet is another important factor and it is suggested that average particle size is not sufficient to characterize a nanofluid due to the non-linear relations involved between particle size and thermal transport. It is also known that particle shape is an effective parameter on the electrical conductivity. The particle size distribution on NDG nanofluids was at 412.4 nm for 60 min ultrasonication time.

Thermal properties analysis

The dependence of thermal conductivity on temperature is presented in Fig. 14, which shows that the effective thermal conductivity increases with increasing temperature and NDG concentration. The enhancement of thermal conductivity for NDG nanofluids is between 22 and 37 %. The principal mechanism of thermal conductivity enhancement can be explained by the stochastic motion of the nanosheets. Based on the literature, there is an interfacial resistance between the nanosheets and base fluid that affects the thermal conductivity of the nanofluids. The suspended nanosheets in the base fluid experience stochastic bombardment from the ambient liquid molecules through the raising of temperature. This causes irregular motion, called Brownian motion (Xuan et al. 2006). Brownian motion is related to nanosheet concentration and fluid temperature (Hemat Esfe et al. 2014). This irregular motion of the nanosheets is induced from micro-mixing or micro-convection inside the base fluid. For these reasons, the energy exchange between the base fluid and the nanosheets is enhanced and the thermal conductivity is enhanced (Xuan et al. 2006).

Rheological behavior analysis

The rheological behaviors of NDG nanofluids are presented in Fig. 15. The viscosity versus shear rate is measured in the range of 20–60 °C and tested over the shear rate range of 0.1–500 s⁻¹. It can be seen that the viscosity reduces between 51.2 and 51.5 % as temperature rises. Thermal movement of molecules, brownian motion intensifies, and intra-molecular

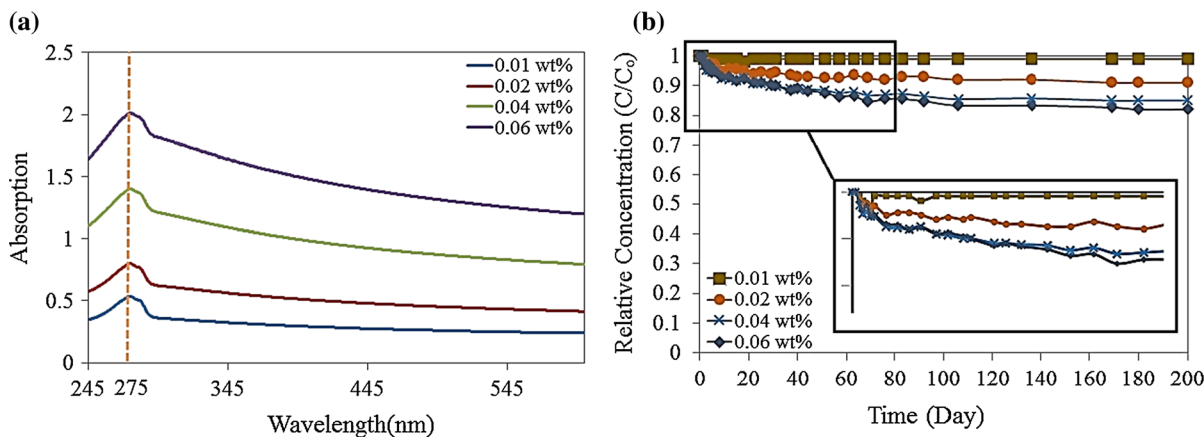


Fig. 13 **a** UV–Vis spectrophotometer of nanofluids at different concentrations and wavelengths and **b** relative supernatant particle concentration of nanofluids with sediment time

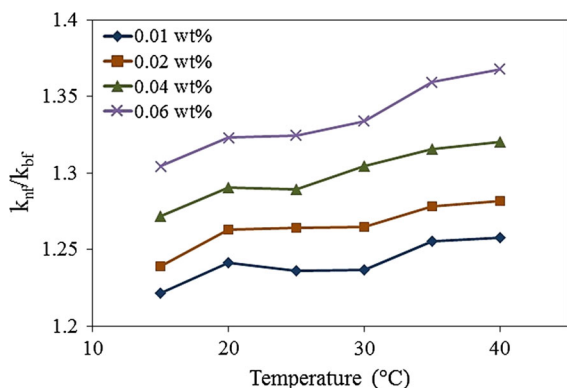


Fig. 14 Effective thermal conductivity of NDG nanofluids as a function of temperature for several concentrations

interactions become weakened with the rise of temperature. Additionally, it is shown that the variation in concentration increases the viscosity; however, other investigated parameters such as temperature and concentration have an important influence on viscosity behavior and heat transfer properties of nanofluids.

Electrical conductivity of aqueous nitrogen-doped graphene nanofluid

Figure 16 shows the electrical conductivity of the NDG nanofluids with respect to weight percentage for different temperatures. As shown Fig. 16, the electrical conductivity increases with increasing the NDG nanosheet concentration. The maximum enhancement of electrical conductivity is 308.16, 667.34, 1311.56, and 1814.96 % at the loading of 0.01, 0.02, 0.04, and

0.06 wt%, respectively. The electrical conductivity also increases almost linearly with temperature, especially at higher concentration. However, the results show that electrical conductivity depends on temperature much less than on NDG concentration.

The increment in electrical conductivity of the NDG nanofluids compare to the base fluid is a consequence of the net charge effect on the NDG nanosheets and the relevant EDL interactions around each particle which is the major importance of colloidal stability of suspensions. As shown in Fig. 17, EDL can exist around each particle and include two parts: (a) an inner region (Stern layer) where the ions are strongly bound and (b) an outer (diffuse) region where they are less firmly associated (Minea and Luciu 2012).

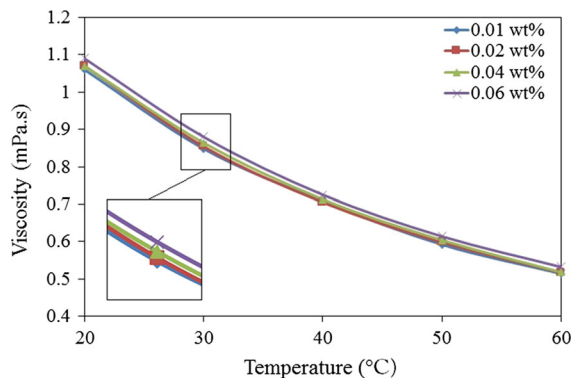


Fig. 15 Viscosity as a function of temperature for several concentrations of NDG nanofluids

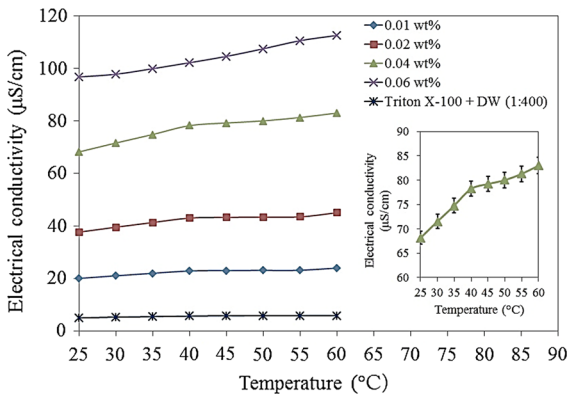


Fig. 16 Electrical conductivity of NDG nanofluids at different temperatures and concentrations. The error bars are not visible because of large range of y axis. *Inset* shows the error bar

When NDG nanosheets are suspended in a base fluid, electric charges develop on the nanosheet surface. Ions of opposite charge to that of the particle surface are attracted, causing the development of a charged diffuse layer surrounding the particles, which is known as EDL as shown in Fig. 17. The ion cloud around the NDG nanosheets, together with the surface charge of NDG, which constitutes the EDL, could enhance the electrical conductivity of the NDG nanofluids. The surface charges are shaped from the nanosheets polarization, when dispersed inside the polar base fluid.

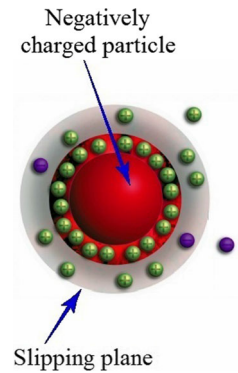
The thickness of interfacial layer (t) often scales as a reciprocal Debye–Huckel parameter, which is described by Eq. (1) (Lee 2007).

$$t = C \left(\sqrt{\varepsilon_0 \varepsilon_r R_0 T / 2000 F^2 I} \right)^{-1}, \tag{1}$$

where ε_0 is vacuum permittivity, R_0 is gas constant, C is constant which depends on temperature, and F is Faraday constant. The remaining properties such as dielectric constant ε_r , temperature T , and ionic strength I are all related to the solution. Additionally, as the primary of the nanosheets gets smaller, the influence of the EDL becomes greater (Lee 2007).

It shows that the thickness of the interfacial layer is dependent on the base fluid and increase in electrophoretic mobility which, consequently, increases the electrical conductivity of the nanofluids. The availability of conducting pathways increases with increase in concentration of nanofluids, thus increasing the overall electrical conductivity. According to

Fig. 17 An example of electric double layer (EDL)



the theory for colloidal stability (DLVO) (Mehrali et al. 2014b), raising of the temperature makes the EDL thicker, which enhanced the effective thermal conductivity of nanofluids (Lee 2007). On the other hand, the viscosity of the nanofluids is strongly dependent on temperature, and this will increase the electrophoretic mobility, which leads to increase the electrical conductivity of nanofluids.

The thickness of the EDL is dependent on the ionic strength of the nanofluids and has a significant effect on electrical conductivity. This effect of ion concentration is captured by the electrokinetic radius (κa), which is the ratio of the particle radius (a) to the thickness of the EDL (κ^{-1}) and is given by Eq. (2) (White et al. 2011).

$$\kappa a = \left[\frac{3ze\zeta}{kT \left(\frac{1}{\phi} - 1 \right)} \right]^{1/2}. \tag{2}$$

As shown in Fig. 7, it is clear that a linearity dependence of electrical conductivity enhancement with temperature is observed with increases of concentration. The possible reason for enhancement of electrical conductivity is that aggregation of nanosheets in the nanofluid is activated by the increased temperature and the electrons are more easily transported through the short conducting paths among the aggregates in the high temperature range. Many researchers including Minea and Luciu (2012) indicated that nanosheet aggregation has both negative and positive effects on the electrical conductivity of the colloidal suspensions, which depends on the temperature and concentration.

Therefore, a simple linear relationship could be developed for the electrical conductivity of NDG at different concentrations as a function of temperature

with purpose interpolating the experimental results, which were fitted by the Eq. (3).

$$\sigma = \alpha + \beta \times (\text{wt}\%). \tag{3}$$

The fitted parameters (α and β) with the correlation coefficient, R^2 , are presented in Table 1. The fitted parameters are functions of temperature are presented in Eqs. (4) and (5).

$$\alpha = \alpha_0 T^n, \tag{4}$$

$$\beta = \beta_0 T^m. \tag{5}$$

The values of the Eqs. (4) and (5) are given in Table 2, and the correlation coefficients, R^2 , for present equations are 0.9835 and 0.9976, respectively.

The ability of the Eqs. (3)–(5) to predict the electrical conductivity value of NDG nanofluids at different temperatures and concentrations were evaluated by the absolute average deviation (AAD).

$$\text{AAD} = \frac{1}{N} \sum_{i=1}^N 100 \left| \frac{\sigma_{\text{exp}} - \sigma_{\text{cal}}}{\sigma_{\text{exp}}} \right|, \tag{6}$$

where σ_{cal} and σ_{exp} represent the predicted and experimental electrical conductivity value, respectively. The AAD of 4.03 % shows that the predicted and experimental values were in a good agreement with each other.

Predictive correlation for electrical conductivity modeling

Maxwell’s model on electrical conductivity in heterogeneous fluid was the first theoretical model to calculate the effective electrical conductivity of nanofluids (Ganguly et al. 2009). Previous studies (Dong et al. 2013; Ganguly et al. 2009) show that the

Table 1 The parameters of Eq. (4)

Temperature (°C)	α ($\mu\text{S}/\text{cm}$)	β ($\mu\text{S}/\text{cm}$)	R^2
25	5.7471	1517.8	0.9990
30	6.5345	1558.5	0.9967
35	6.7645	1595.3	0.9945
40	7.1147	1636.7	0.9918
45	7.2295	1674.9	0.9934
50	7.2438	1721.3	0.9955
55	7.6464	1773.7	0.9967
60	7.8515	1802.9	0.9963

Maxwell model on the electrical conductivity in nanofluid is not only associated with the physical properties but also relates to some other physicochemical properties including the agglomeration, size and shape of the nanosheets, the electrophoresis, the EDL, and the Brownian motion of nanosheets. When the concentration of nanosheets is low, the aggregation of nanosheets is not serious; the nanofluid can be treated as a monodisperse system. The mobility of the charged nanosheets caused by the Brownian motion increases with the increasing of temperature; thus, the electrical conductivity of the nanofluid is enlarged. The effect of nanosheet aggregation on the electrical conductivity is an active research area till today.

Maxwell’s model for nanofluids was the first theoretical method, which was used to calculate the effective electrical conductivity. The Maxwell’s model predicts the effective conductivity of nanofluids (σ_{eff}), electrical conductivity of the base fluid (σ_{bf}), electrical conductivity of the nanosheets (σ_{np}), and the volume fraction ϕ of the nanosheets (Ganguly et al. 2009). Equation (7) illustrated that the Maxwell’s model on the effective conductivity (σ_{eff}) of nanofluids.

$$\frac{\sigma_{\text{eff}}}{\sigma_{\text{bf}}} = 1 + \frac{3(\alpha - 1)\phi}{(\alpha + 2) - (\alpha - 1)\phi}, \tag{7}$$

where $\alpha = \frac{\sigma_{\text{np}}}{\sigma_{\text{bf}}}$ is the conductivity ratio of the two phases. Based on the literature, Maxwell’s model depends on the conducting nature of the base fluid and the nanosheets and this model could be simplified, as shown in Eqs. (8)–(10).

$$\frac{\sigma_{\text{eff}}}{\sigma_{\text{bf}}} = 1 - \frac{3}{2}\phi, \quad \text{for } \sigma_{\text{np}} \ll \sigma_{\text{bf}} \text{ (insulating particles)}, \tag{8}$$

$$\frac{\sigma_{\text{eff}}}{\sigma_{\text{bf}}} = 1, \quad \text{for } \sigma_{\text{np}} = \sigma_{\text{bf}} \text{ (equal conductivity)}. \tag{9}$$

$$\frac{\sigma_{\text{eff}}}{\sigma_{\text{bf}}} = 1 + 3\phi, \quad \text{for } \sigma_{\text{np}} \gg \sigma_{\text{bf}} \text{ (highly conducting particles)}. \tag{10}$$

Table 2 The fitting parameters of Eqs. (5) and (6)

α_0	n	β_0	m
2.176	0.3144	788.62	0.2002

Some researchers verified the applicability of the Maxwell’s model by experimental data for dilute suspensions ($\phi \ll 1$) with large particles (particle size larger than tens of micrometers). They found that in this situation, the slope of the relative electrical conductivity curve for insulating nanosheets (i.e., alumina nanosheets have very poor electrical conductivity characteristics) has a negative value (-1.5) and it is expected that the mixture’s electrical conductivity is reduced. On the other hand, the Maxwell’s model is acceptable for the nanosheets with spherical and monodisperse shape, which is the main limitation of this model. Ganguly et al. (2009) found that the measured electrical conductivity of the Al_2O_3 increases linearly with volume fraction of the nanosheets. They have shown that the theoretical model and measurements for dispersions with large size (micrometer or larger) agree well and the electrical conductivity increases in nanosheet-fluid mixtures. The enhancement of electrical conductivity of nanofluids is effected by different parameters including physical properties of fluid and nanosheets. The effective electrical conductivity of nanosheets in a base fluid exhibits a complex dependence on ionic concentrations, volume fraction, the EDL characteristics, and other physicochemical properties, which are not effectively captured by the standard models.

As stated earlier, according to the theory of colloid and surface chemistry, there is an EDL around each particle surface (O’Dwyer 1973). The ion cloud around the nanosheets, together with surface charge constitutes the EDL, which increased the conduction through the electrophoretic transactions. Generally, the nanosheet suspensions have a zeta potential (ζ) relative to the base fluid at different pHs, and when an electrical field is applied to the nanofluids, the charged nanosheets will move towards the electrode and this is due to the electrophoretic conductivity of nanosheets; the electron attachment on the particle could be expressed as Eq. (11).

$$q = 4\pi\epsilon_r\epsilon_0r\zeta. \tag{11}$$

By the assumption that the nanosheets have a uniform velocity under the joint function of viscous force and electric force, the electrophoretic conductivity can be calculated by Eq. (12).

$$\sigma_E = \frac{8\pi n_0 \epsilon_r^2 \epsilon_0^2 r^2}{3\mu}, \tag{12}$$

$$n_0 = 3\phi/4\pi r^3, \tag{13}$$

where n_0 is the number of nanosheets per unit volume, $\mu = \nu\rho$ is the dynamic viscosity of the nanofluids. ν and ρ are the kinematic viscosity and density of the nanofluid. ϵ_r and ϵ_0 are the dielectric constant of the vacuum and the relatively dielectric constant of the nanosheets, respectively. Hence, Eqs. (12) and (13) can be expressed as Eq. (14).

$$\sigma_E = \frac{2\phi\epsilon_r^2\epsilon_0^2r^2}{\mu r^2}. \tag{14}$$

If the n_0 , ϵ_r , ζ , and r remain unchanged in the Eq. (14), the value of $\sigma_E\mu$ also remains constant. Walden law shows that the electrical conductivity and viscosity of nanofluids changed with temperature and product of σ and η will remain constant in the nanofluids (Bailar and Auten 1934). The zeta potential and dynamic viscosity of nanofluids are affected by the concentration of nanofluid. Additionally, the dynamic viscosity will increase with the rise in the concentrations of the nanosheets, while the zeta potential will decrease with the concentration because the EDL is suppressed at higher concentrations (Dong et al. 2013). The variation of dynamic viscosity of the nanofluid can be described by Eq. (14), when the volume concentration of the nanofluid is lower than 10 % (Dong et al. 2013).

$$\mu = \mu_{bf}(1 + \eta\phi + k_H\phi^2). \tag{15}$$

In this equation, η is the intrinsic viscosity and k_H is Huggins’ coefficient. The value of η and k_H is 2.5 and 6.5, respectively (Aladag et al. 2012). On the other hand, fluid mechanics laws show that the viscosity of the fluid varies with particles’ concentrations, pressure, and temperature. Since the pressure has only small effect on the viscosity, the relationship between the viscosity and temperature can be expressed as Eq. (15) (Crowe et al. 2005).

$$\mu = \mu_{nf}e^{-\lambda(T-T_0)}, \tag{16}$$

where μ_{nf} is the dynamic viscosity of the nanofluid at temperature T_0 and λ is the decreasing rate of the viscosity when the temperature is increasing. The

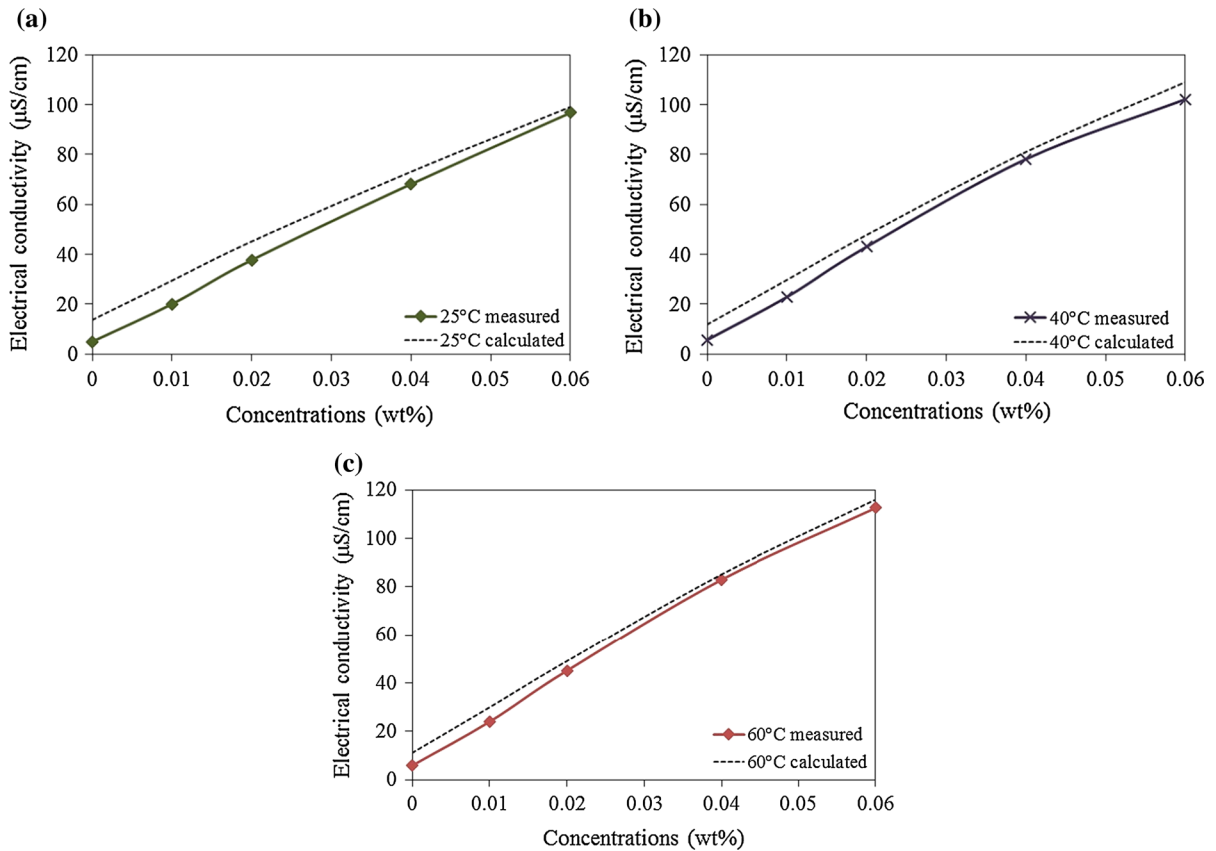


Fig. 18 The experimental and theoretical electrical conductivity of the NDG nanofluids as a function of concentration at three different temperatures: **a** 25 °C, **b** 40 °C, and **c** 60 °C

electrophoresis conductivity of the nanofluid is obtained by substituting of Eqs. (11)–(16).

$$\sigma_E = \frac{2\phi\epsilon_r^2\epsilon_0^2r^2}{\rho\nu(1 + 2.5\phi + 6.5\phi^2)} \times e^{-\lambda(T-T_0)}. \quad (17)$$

The total electrical conductivity of nanofluids is calculated based on the Maxwell’s model and dynamic electrical conductivity, which is caused by the electrophoresis of the nanosheets. Finally, the new electrical conductivity model is defined as Eq. (17).

$$\begin{aligned} \sigma &= \sigma_M + \sigma_E \\ &= \frac{\sigma_{np} + 2\sigma_{bf} - 2\phi(\sigma_{nf} - \sigma_{np})}{\sigma_{np} + 2\sigma_{nf} + \phi(\sigma_{nf} - \sigma_{np})} \\ &\quad + \frac{2\phi\epsilon_r^2\epsilon_0^2r^2}{\rho\nu(1 + 2.5\phi + 6.5\phi^2)} \times e^{-\lambda(T-T_0)}. \end{aligned} \quad (18)$$

Base on the literature, electrical conductivity of NDG is about 1000 S/m. Figure 18 represents the calculated and measured electrical conductivity as a

function of concentration at different temperatures. It is found that the experimental data agree well with the theoretical value when the concentration is between 0.01 and 0.06 wt%. However, the experimental data could be underestimated at smaller weight percentage and at large weight percentage is overestimated. The reason is, while the concentrations of nanofluid are too low, the nanosheets electrophoretic motion should overcome percolation threshold, but the Maxwell’s model does not take this factor into consideration (Dong et al. 2013). On the other hand, when the concentrations of nanosheets becomes larger, the main deviation of the Maxwell’s model does not consider the agglomeration effects.

According to EDL theory, the electrical conductivity of nanofluids increases due to short conducting paths by aggregate contact of the nanosheets. It is notable that Debye length is inversely proportional to the root square of the electrical conductivity, and the Debye length in a low conducting fluid is very large.

On the other hand, it is interesting to observe that the EDL not only enhances the electrical conductivity of the nanofluid but also plays a significant role in the electrical conduction. This may be due to the fact that in high concentration and nanoscale solid–fluid suspension, the EDLs' distribution and interaction have changed.

Conclusions

Highly stable aqueous NDG nanofluids were prepared by a two-step method in a 0.025 wt% Triton X-100 (as a surfactant) aqueous solution as a base. The electrical conductivity was measured at different concentrations and temperatures and it was found that electrical conductivities increased almost linearly with increase in concentration of nanofluids up to 1814.96 %. The experimental results show that electrical conductivity depends on temperature much less than on NDG concentration. A linear regression analysis on NDG nanofluid, based on the concentrations and temperature has been applied to develop an empirical relationship for the electrical conductivity. The present analysis indicates the relative influence of these two parameters on the electrical conductivity enhancement. The results show that the electrical conductivity of NDG does not follow the traditional Maxwell model. In this study, by considering the electrophoresis of the NDG nanosheets, a straight forward electrical conductivity model is established. We believe that this type of nanofluids could potentially increase their applicability in technologies, which require high electrical conductive fluids.

Acknowledgments This research work has been financially supported by the Ministry of High Education (MOHE) of Malaysia under Grant No. UM.C/625/1/HIR/MOHE/ENG/21, UMRG Grant RP021-2012A, and Malaysian FRGS National Grant FP007/2013A.

Conflict of interest The authors declare that they have no competing interests.

References

- Akhavan O (2010) The effect of heat treatment on formation of graphene thin films from graphene oxide nanosheets. *Carbon* 48:509–519. doi:[10.1016/j.carbon.2009.09.069](https://doi.org/10.1016/j.carbon.2009.09.069)
- Akhavan O, Ghaderi E (2012) *Escherichia coli* bacteria reduce graphene oxide to bactericidal graphene in a self-limiting manner. *Carbon* 50:1853–1860. doi:[10.1016/j.carbon.2011.12.035](https://doi.org/10.1016/j.carbon.2011.12.035)
- Aladag B, Halefadi S, Doner N, Maré T, Duret S, Estellé P (2012) Experimental investigations of the viscosity of nanofluids at low temperatures. *Appl Energy* 97:876–880. doi:[10.1016/j.apenergy.2011.12.101](https://doi.org/10.1016/j.apenergy.2011.12.101)
- Aravind SJ, Baskar P, Baby TT, Sabareesh RK, Das S, Ramaprabhu S (2011) Investigation of structural stability, dispersion, viscosity, and conductive heat transfer properties of functionalized carbon nanotube based nanofluids. *J Phys Chem C* 115:16737–16744
- Azizi-Toupkanloo H, Goharshadi EK, Nancarrow P (2013) Structural, electrical, and rheological properties of palladium/silver bimetallic nanoparticles prepared by conventional and ultrasonic-assisted reduction methods. *Adv Powder Technol* 25:801–810. doi:[10.1016/j.appt.2013.11.015](https://doi.org/10.1016/j.appt.2013.11.015)
- Bailar JC, Auten RW (1934) The stereochemistry of complex inorganic compounds. I. The Walden inversion as exhibited by diethylenediaminocobaltic compounds. *J Am Chem Soc* 56:774–776. doi:[10.1021/ja01319a004](https://doi.org/10.1021/ja01319a004)
- Banerjee N, Krupanidhi SB (2010) Facile hydrothermal synthesis and observation of bubbled growth mechanism in nano-ribbons aggregated microspherical Covellite blue-phosphor. *Dalton Trans* 39:9789–9793. doi:[10.1039/C0DT00386G](https://doi.org/10.1039/C0DT00386G)
- Blanton TN, Majumdar D (2012) X-ray diffraction characterization of polymer intercalated graphite oxide. *Powder Diffraction* 27:104–107. doi:[10.1017/S0885715612000292](https://doi.org/10.1017/S0885715612000292)
- Chakraborty S, Padhy S (2008) Anomalous electrical conductivity of nanoscale colloidal suspensions. *ACS Nano* 2:2029–2036
- Crowe CT, Elger DF, Roberson JA, Crowe CT, Crowe CT (2005) *Engineering fluid mechanics*, vol 9. Wiley, Hoboken
- Cruz RC, Reinshagen J, Oberacker R, Segadães AM, Hoffmann MJ (2005) Electrical conductivity and stability of concentrated aqueous alumina suspensions. *J Colloid Interface Sci* 286:579–588
- Dong M, Shen LP, Wang H, Wang HB, Miao J (2013) Investigation on the electrical conductivity of transformer oil-based AlN nanofluid. *J Nanomater*. doi:[10.1155/2013/842963](https://doi.org/10.1155/2013/842963)
- Fang F, Zhang Y (2005) DC electrical conductivity of Au nanoparticle/chloroform and toluene suspensions. *J Mater Sci* 40:2979–2980
- Ganguly S, Sikdar S, Basu S (2009) Experimental investigation of the effective electrical conductivity of aluminum oxide nanofluids. *Powder Technol* 196:326–330. doi:[10.1016/j.powtec.2009.08.010](https://doi.org/10.1016/j.powtec.2009.08.010)
- Goharshadi EK, Azizi-Toupkanloo H (2013) Silver colloid nanoparticles: ultrasound-assisted synthesis, electrical and rheological properties. *Powder Technol* 237:97–101
- Goharshadi E, Azizi-Toupkanloo H, Karimi M (2014) Electrical conductivity of water-based palladium nanofluids. *Microfluid Nanofluid* 18:1–6. doi:[10.1007/s10404-014-1465-0](https://doi.org/10.1007/s10404-014-1465-0)
- Guo H-L, Su P, Kang X, Ning S-K (2013) Synthesis and characterization of nitrogen-doped graphene hydrogels by

- hydrothermal route with urea as reducing-doping agents. *J Mater Chem A* 1:2248–2255. doi:[10.1039/C2TA00887D](https://doi.org/10.1039/C2TA00887D)
- Hemmat Esfe M, Saedodin S, Mahian O, Wongwises S (2014) Thermophysical properties, heat transfer and pressure drop of COOH-functionalized multi walled carbon nanotubes/water nanofluids. *Intern Commun Heat Mass Transf* 58:176–183. doi:[10.1016/j.icheatmasstransfer.2014.08.037](https://doi.org/10.1016/j.icheatmasstransfer.2014.08.037)
- Hernandez Y et al (2008) High-yield production of graphene by liquid-phase exfoliation of graphite. *Nat Nano* 3:563–568. http://www.nature.com/nnano/journal/v3/n9/supinfo/nnano.2008.215_S1.html
- Kalteh M, Abbassi A, Saffar-Avval M, Harting J (2011) Eulerian-Eulerian two-phase numerical simulation of nanofluid laminar forced convection in a microchannel. *Int J Heat Fluid Flow* 32:107–116
- Kole M, Dey T (2013) Investigation of thermal conductivity, viscosity, and electrical conductivity of graphene based nanofluids. *J Appl Phys* 113:084307
- Lee D (2007) Thermophysical properties of interfacial layer in nanofluids. *Langmuir* 23:6011–6018. doi:[10.1021/la063094k](https://doi.org/10.1021/la063094k)
- Lin Y-C, Lin C-Y, Chiu P-W (2010) Controllable graphene N-doping with ammonia plasma. *Appl Phys Lett* 96:133110–133113
- Lisunova MO, Lebovka NI, Melezhyk OV, Boiko YP (2006) Stability of the aqueous suspensions of nanotubes in the presence of nonionic surfactant. *J Colloid Interface Sci* 299:740–746
- Liu J, Takeshi D, Orejon D, Sasaki K, Lyth SM (2014) Defective nitrogen-doped graphene foam: a metal-free, non-precious electrocatalyst for the oxygen reduction reaction in acid. *J Electrochem Soc* 161:F544–F550
- Long D, Li W, Ling L, Miyawaki J, Mochida I, Yoon S-H (2010) Preparation of nitrogen-doped graphene sheets by a combined chemical and hydrothermal reduction of graphene oxide. *Langmuir* 26:16096–16102. doi:[10.1021/la102425a](https://doi.org/10.1021/la102425a)
- Maxwell JC (1881) A treatise on electricity and magnetism, vol 1. Clarendon Press, Oxford
- Maxwell JC, Thompson JJ (1904) A treatise on electricity and magnetism vol 2. Clarendon Press, Oxford
- Mehrali M, Latibari ST, Mehrali M, Mahlia TMI, Metselaar HSC (2013a) Preparation and properties of highly conductive palmitic acid/graphene oxide composites as thermal energy storage materials. *Energy* 58:628–634. doi:[10.1016/j.energy.2013.05.050](https://doi.org/10.1016/j.energy.2013.05.050)
- Mehrali M, Latibari ST, Mehrali M, Metselaar HSC, Silakhori M (2013b) Shape-stabilized phase change materials with high thermal conductivity based on paraffin/graphene oxide composite. *Energy Convers Manag* 67:275–282. doi:[10.1016/j.enconman.2012.11.023](https://doi.org/10.1016/j.enconman.2012.11.023)
- Mehrali M et al (2014a) Synthesis, mechanical properties and in vitro biocompatibility with osteoblasts of calcium silicate-reduced graphene oxide composites. *ACS Appl Mater Interfaces* 6:3947–3962
- Mehrali M, Sadeghinezhad E, Latibari ST, Kazi SN, Mehrali M, Zubir MNBM, Metselaar HSC (2014b) Investigation of thermal conductivity and rheological properties of nanofluids containing graphene nanoplatelets. *Nanoscale Res Lett* 9:1–12
- Mehrali M, Latibari ST, Mehrali M, Mahlia TMI, Sadeghinezhad E, Metselaar HSC (2014c) Preparation of nitrogen-doped graphene/palmitic acid shape stabilized composite phase change material with remarkable thermal properties for thermal energy storage. *Appl Energy* 135:339–349. doi:[10.1016/j.apenergy.2014.08.100](https://doi.org/10.1016/j.apenergy.2014.08.100)
- Mehrali M, Sadeghinezhad E, Latibari ST, Mehrali M, Togun H, Zubir MNM, Metselaar HSC (2014d) Preparation, characterization, viscosity, and thermal conductivity of nitrogen-doped graphene aqueous nanofluids. *J Mater Sci* 49:7156–7171. doi: [10.1007/s10853-014-8424-8](https://doi.org/10.1007/s10853-014-8424-8)
- Minea AA, Luciu RS (2012) Investigations on electrical conductivity of stabilized water based Al₂O₃ nanofluids. *Microfluid Nanofluid* 13:977–985
- Ohshima H, Furusawa K (eds) (1998) Electrical phenomena at interfaces: fundamentals: measurements, and applications, vol 76. CRC Press, Boca Raton
- O'Dwyer JJ (1973) The theory of electrical conduction and breakdown in solid dielectrics. Clarendon Press, Oxford
- Reddy ALM, Srivastava A, Gowda SR, Gullapalli H, Dubey M, Ajayan PM (2010) Synthesis of nitrogen-doped graphene films for lithium battery application. *ACS Nano* 4:6337–6342. doi:[10.1021/nn101926g](https://doi.org/10.1021/nn101926g)
- Sadeghinezhad E, Mehrali M, Latibari ST, Mehrali M, Kazi SN, Oon S, Metselaar HSC (2014) Experimental investigation of convective heat transfer using graphene nanoplatelet based nanofluids under turbulent flow conditions. *Ind Eng Chem Res* 53:12455–12465. doi:[10.1021/ie501947u](https://doi.org/10.1021/ie501947u)
- Safaei MR, Togun H, Vafai K, Kazi SN, Badarudin A (2014) Investigation of heat transfer enhancement in a forward-facing contracting channel using FMWCNT nanofluids. *Numer Heat Transf A* 66:1321–1340. doi:[10.1080/10407782.2014.916101](https://doi.org/10.1080/10407782.2014.916101)
- Sheng Z-H, Shao L, Chen J-J, Bao W-J, Wang F-B, Xia X-H (2011) Catalyst-free synthesis of nitrogen-doped graphene via thermal annealing graphite oxide with melamine and its excellent electrocatalysis. *ACS Nano* 5:4350–4358. doi:[10.1021/nn103584t](https://doi.org/10.1021/nn103584t)
- Togun H, Safaei MR, Sadri R, Kazi SN, Badarudin A, Hooman K, Sadeghinezhad E (2014) Numerical simulation of laminar to turbulent nanofluid flow and heat transfer over a backward-facing step. *Appl Math Comput* 239:153–170. doi:[10.1016/j.amc.2014.04.051](https://doi.org/10.1016/j.amc.2014.04.051)
- Usachov D et al (2011) Nitrogen-doped graphene: efficient growth, structure, and electronic properties. *Nano Lett* 11:5401–5407. doi:[10.1021/nl2031037](https://doi.org/10.1021/nl2031037)
- Vinayan BP, Ramaprabhu S (2013) Facile synthesis of SnO₂ nanoparticles dispersed nitrogen doped graphene anode material for ultrahigh capacity lithium ion battery applications. *J Mater Chem A* 1:3865–3871. doi:[10.1039/C3TA01515G](https://doi.org/10.1039/C3TA01515G)
- Wei D, Liu Y, Wang Y, Zhang H, Huang L, Yu G (2009) Synthesis of N-doped graphene by chemical vapor deposition and its electrical properties. *Nano Lett* 9:1752–1758
- White SB, Shih AJ-M, Pipe KP (2011) Investigation of the electrical conductivity of propylene glycol-based ZnO nanofluids. *Nanoscale Res Lett* 6:1–5
- Wong K-F, Bhshkar T (2006) Transport properties of alumina nanofluids. In: ASME 2006 international mechanical engineering congress and exposition, American Society of Mechanical Engineers, pp 251–260
- Wu P, Qian Y, Du P, Zhang H, Cai C (2012) Facile synthesis of nitrogen-doped graphene for measuring the releasing

- process of hydrogen peroxide from living cells. *J Mater Chem* 22:6402–6412. doi:[10.1039/C2JM16929K](https://doi.org/10.1039/C2JM16929K)
- Xuan Y, Li Q, Zhang X, Fujii M (2006) Stochastic thermal transport of nanoparticle suspensions. *J Appl Phys* 100:043507. doi:[10.1063/1.2245203](https://doi.org/10.1063/1.2245203)
- Yousefi T, Shojaeizadeh E, Veysi F, Zinadini S (2012) An experimental investigation on the effect of pH variation of MWCNT-H₂O nanofluid on the efficiency of a flat-plate solar collector. *Sol Energy* 86:771–779